Research Article

Vibration Suppression of Bolter Miner Employing Dynamic Vibration Absorber

Ang Li [ID],[1] Bukang Wang,[1,2,3] Teng Wang,[1,2,3] Zhifu Guo,[1,2,3] and Zhaokun Yan[4]

[1]*China Coal Research Institute, Beijing, China*
[2]*CCTEG Taiyuan Research Institute Co., Ltd, Taiyuan, China*
[3]*China National Engineering Laboratory for Coal Mining Machinery, Taiyuan, China*
[4]*Taiyuan University of Technology, Taiyuan, China*

Correspondence should be addressed to Ang Li; liangccteg@163.com

The bolter miner is a critical piece of equipment in the rapid set of tunneling equipment, and the load generated during coal cutting may lead to excessive vibration of the equipment and reduce its reliability. In order to reduce the vibration response of the bolter miner, this paper proposes the installation of a dynamic vibration absorber (DVA) inside the cutting arm of the bolter miner. A five-degree-of-freedom dynamics model was developed, and the cutting part was regarded as two rigid bodies flexibly connected by a rotating spring. The model's accuracy was verified based on the field test results, and the error was within 7%. It was found that the cutting caused the first-order modal vibration, and the DVA was placed in the cavity of the cutting arm to control the modal vibration of this order. To minimize the vibration, a coupled dynamics model between the DVA and bolter miner was developed, and the DVA parameters were optimized. The results showed that the acceleration RMS and peak values of the cutting part were reduced by 12% and 30.1%, respectively; the acceleration RMS and peak values of the main frame were reduced by 6.5% and 17%, respectively, and the fatigue life of the cutting arm was increased by 34.2%.

1. Introduction

Coal mining in China is mainly underground, and new tunneling can reach 12,000 km per year [1]. In order to ensure safe and rapid roadway excavation, many coal mines have introduced rapid excavation equipment with the bolter miner as the core. The advantage of the bolter miner is that the functions of tunneling, support, and transportation are concentrated into an integral system [2]. Due to the rock-breaking method of the cutting head, the bolter miner is subjected to this large load during the operation, which leads to strong vibration of the equipment. Excessive vibration can cause excessive stress and discomfort to workers, while accelerating fatigue damage to key components such as cutting arms, reducing tunnel boring efficiency, and increasing maintenance costs [3].

Tunneling equipment also includes a roadheader as well as continuous miners. Many scholars have studied the

vibration suppression of tunneling equipment. The literature [4] established a dynamics model of a roadheader boom, and the results of its analysis showed that the resonance problem is difficult to eliminate due to the wide distribution of load frequencies and the constant variation of the boom's intrinsic frequency with the change of the boom's position. Therefore, the number of cutting head cutter teeth and their arrangement were optimized to avoid resonance. In the literature [5], the continuous miner model was established by the finite element method. The first eight orders of modal vibration were calculated. The parameters of the elastic element and the cutting head speed were optimized to reduce the displacement of the cutting head and the main frame. It is necessary to avoid resonance in the research and development stage through the reasonable design of machine structure parameters and motion parameters, but in practice, the dynamics parameters used in the simulation are often inconsistent with the actual, which reduces the

vibration reduction capability [6]. Also, for the tunneling equipment in service, how to reduce its vibration amplitude failed to propose a corresponding solution.

The main contribution of this paper is to apply the theory of dynamic vibration absorption to the vibration reduction of the bolter miner. A standard passive dynamic vibration absorber (DVA) is a mass connected to the primary structure by a linearly elastic spring and a viscous dashpot [7, 8]. The researchers commonly state that the passive DVA is the simplest and most robust [9]. Several types of DVA have been developed to meet various needs (in some fields, DVA is also called tuned mass damper (TMD)): TMD-inerter (TMDI) compounding the conventional TMD with an inerter device. The inerter in the introduced TMDI configuration provides a "mass amplification effect" [10]. Particle dampers are robust and reliable and can be used to dampen vibrations in lightly damped structures, especially in harsh environments [11]. The tuned liquid column damper (TLCD) serves as a vibration damper that not only suppresses vibration in buildings but also serves as a water storage facility for buildings [12]. DVA is a well-known technology with many structural and wind engineering applications. Some famous buildings, such as the Citigroup Tower in New York City, the 101 Tower in Taipei, the Aspire Tower in Doha, Qatar, and the Shanghai World Financial Center in Shanghai, China, have deployed DVAs [13]. DVA is usually placed in the top nacelle to handle the large displacement amplitude due to the first-order modal shape of the wind turbine tower [14]. A large body of literature has verified the ability of DVA for vibration reduction. However, it is the first study to apply DVA for the antiresonance design of tunneling equipment.

This paper systematically studies the application of DVA in bolter miner vibration reduction with the EJM340 bolter miner as the research object. A five-degree-of-freedom model was used. The cutting load was obtained based on the DEM-MFBD bidirectional coupling technique. Field tests were conducted to verify the model's accuracy and determine the primary frequency of bolter miner vibration. The DVA is placed in the cavity of the cutting arm to absorb the first-order modal vibrations, and the parameters of the DVA are optimized by establishing an objective function. Finally, the performance of DVA was comprehensively evaluated and verified. The structure of this paper is organized as follows. Section 2 presents the dynamic equations of the bolter miner. Section 3 calculates the cutting load. Section 4 verifies the accuracy of the dynamics model and obtains the main vibration frequencies through field tests. Section 5 establishes the coupled dynamics model of the bolter miner and DVA and optimizes the DVA. Section 6 validates the performance of DVA. The main conclusions are drawn in Section 7.

2. Bolter Miner

2.1. Equations of Motion. An EJM340 bolter miner was used as the research object, and its technical parameters are listed in Table 1. The bolter miner consists of a main frame and cutting part, and the cutting part consists of a cutting arm and cutting head. To calculate the stiffness, damping, and mass parameters of the TMD, a simple and accurate mathematical model of the bolter miner must be established, as shown in Figure 1.

According to the working environment and structural form of the bolter miner, the multibody dynamics model is simplified and assumed as follows:

(1) Because the cutting head is symmetrically distributed and the axial forces cancel each other out, the vibration in the axial direction is neglected.

(2) Considering point B as a hinge, the cutting part is divided into two rigid bodies, cutting part 1 and cutting part 2, respectively, and a torsion spring is introduced to represent the resistance to the bending deformation of the beam.

(3) Assume that a massless elastic element connects the parts of the bolter miner and that the damping between all parts is viscous damping.

The dynamic model of the bolter miner was described by five degrees of freedom, as shown in Table 2. Kinetic equations were then established.

$$\mathbf{M\ddot{X}} + \mathbf{C\dot{X}} + \mathbf{KX} = \mathbf{Q}, \tag{1}$$

where $X = [x\ y\ \theta_b\ \theta_{c1}\ \theta_{c2}]\ T$, and M, K, and C are the mass, damping, and stiffness matrices, respectively. Q is the vector of the external forces, as described in Section 3.

The mass matrix M is

$$\mathbf{M} = \begin{vmatrix} m_b + m_{c1} + m_{c2} & 0 & 0 & m_{c1}l_{cm}\sin\varphi_1 + m_{c2}l_{c1}\sin\varphi_1 & m_{c2}l_{c2}\sin\varphi_1 \\ 0 & m_b + m_c + m_{c2} & m_{c1}l_{b4} + m_{c2}l_{b4} & m_{c1}l_{cm}\cos\varphi_1 + m_{c2}l_{c1}\cos\varphi_1 & m_{c2}l_{c2}\cos\varphi_1 \\ 0 & m_{c1}l_{b4} + m_{c2}l_{b4} & I_b + m_{c1}l_{b4}^2 + m_{c2}l_{b4}^2 & m_{c1}l_{b4}l_{c1}\cos\varphi_1 + m_{c2}l_{b4}l_{c1}\cos\varphi_1 & m_{c2}l_{b4}l_{c2}\cos\varphi_1 \\ m_c l_{cm}\sin\varphi_1 + m_{c2}l_{c1}\sin\varphi_1 & m_c l_{cm}\cos\varphi_1 + m_{c2}l_{c1}\cos\varphi_1 & m_{c1}l_{b4}l_{c1}\cos\varphi_1 + m_{c2}l_{b4}l_{c1}\cos\varphi_1 & I_{c1} + m_{c1}l_{cm}^2 + m_{c2}l_{c1}^2 & m_{c2}l_{c1}l_{c2} \\ m_{c2}l_{c2}\sin\varphi_1 & m_{c2}l_{c2}\cos\varphi_1 & m_{c2}l_{b4}l_{c2}\cos\varphi_1 & m_{c2}l_{c1}l_{c2} & I_{c2} + m_{c2}l_{c2}^2 \end{vmatrix}. \tag{2}$$

The stiffness matrix K is

TABLE 1: Bolter miner machine parameters.

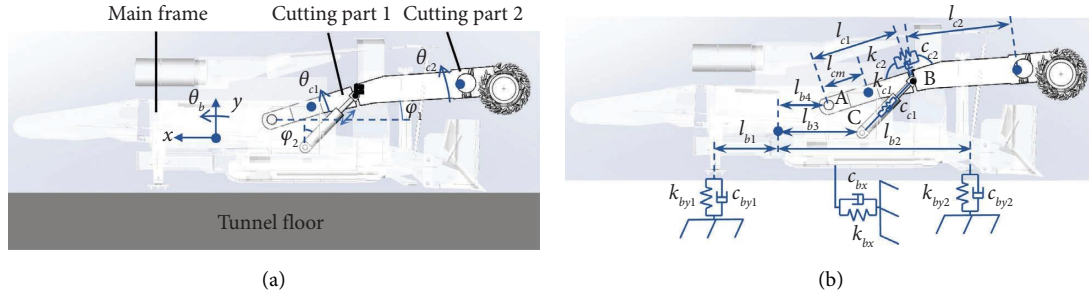| Parameters	Value
Overall weight (t)	103
Dimension ($L \times W \times H$) (mm)	$11640 \times 5000 \times 2600$
Cutting head diameter (mm)	1150
Cutting head width (mm)	5200
Total power (kW)	742
Ground pressure (MPa)	0.27

(a)

(b)

FIGURE 1: Bolter miner: (a) 5-DOF mode and (b) equivalent spring model.

TABLE 2: The five DOF of the system.

Definition	DOF
Translation of the main frame along the x-axis	x
Translation of the main frame along the y-axis	y
Rotation of the main frame around the center of gravity	θ_b
Rotation of the cutting part 1 around the hinge point A	θ_{c1}
Rotation of the cutting part 2 around the hinge point B	θ_{c2}

$$\mathbf{K} = \begin{vmatrix} k_{bx} & 0 & 0 & 0 & 0 \\ 0 & k_{by1} + k_{by2} & k_{by2}l_{b2} - k_{by1}l_{b1} & 0 & 0 \\ 0 & k_{by2}l_{b2} - k_{by1}l_{b1} & k_{by2}l_{b2}^2 + k_{by1}l_{b1}^2 + k_{c1}(l_{b4} - l_{b3})^2\cos^2\varphi_2 & k_{c1}(l_{b4} - l_{b3})l_{c1}\cos(\varphi_1 + \varphi_2) & 0 \\ 0 & 0 & k_{c1}(l_{b4} - l_{b3})l_{c1}\cos(\varphi_1 + \varphi_2) & k_{c1}l_{c1}^2\cos^2(\varphi_1 + \varphi_2) + k_{c2} & -k_{c2} \\ 0 & 0 & 0 & -k_{c2} & k_{c2} \end{vmatrix}. \tag{3}$$

The damping matrix C is

$$\mathbf{C} = \begin{vmatrix} c_{bx} & 0 & 0 & 0 & 0 \\ 0 & c_{by1} + c_{by2} & c_{by2}l_{b2} - c_{by1}l_{b1} & 0 & 0 \\ 0 & c_{by2}l_{b2} - c_{by1}l_{b1} & c_{by2}l_{b2}^2 + c_{by1}l_{b1}^2 + c_{c1}(l_{b4} - l_{b3})^2\cos^2\varphi_2 & c_{c1}(l_{b4} - l_{b3})l_{c1}\cos(\varphi_1 + \varphi_2) & 0 \\ 0 & 0 & c_{c1}(l_{b4} - l_{b3})l_{c1}\cos(\varphi_1 + \varphi_2) & c_{c1}l_{c1}^2\cos^2(\varphi_1 + \varphi_2) + c_{c2} & -c_{c2} \\ 0 & 0 & 0 & -c_{c2} & c_{c2} \end{vmatrix}, \tag{4}$$

where m_b, m_{c1}, and m_{c2} are the masses of the main frame and cutting part 1 and cutting part 2, respectively. I_b, I_{c1}, and I_{c2} are the moments of inertia about the center of gravity of the main frame and cutting part 1 and cutting part 2, respectively. k_{by1} and c_{by1} are the stiffness and damping

between the rear of the main frame and the tunnel floor in the y direction, respectively. k_{by2} and c_{by2} are the stiffness and damping between the front of the main frame and the tunnel floor in the y direction, respectively. k_x and c_x are the stiffness and damping between the main frame and tunnel

floor in the x direction, respectively. k_{c1} and c_{c1} are the stiffness and damping of the cutting cylinder, respectively. k_{c2} and c_{c2} are the rotation stiffness and damping of the cutting part, respectively. l_{b1} and l_{b2} are the distances between the rear and front of the main frame and its center of gravity in the x direction, respectively. l_{b3} is the distance between the hinge point C and the gravity of the main frame in the x direction. l_{b4} is the distance between the hinge point A and the gravity of the main frame in the x direction. l_{c1} is the distance between the hinge point A and the hinge point B. l_{c2} is the distance between hinge point B and the center of gravity of cutting part 2. l_{cm} is the distance between hinge point B and the center of gravity of cutting part 2. φ_1 is the angle between the cutting part and the x direction. φ_2 is the angle between the cutting cylinder and the y direction.

The values of the parameters are summarized in Table 3.

2.2. Modal Analysis.

The model of the system was analyzed to study the vibration mechanism of the system. Based on the M and K matrices, the natural frequencies of the system and the corresponding vibration shapes can be calculated and are listed in Table 4. The first and second modes are the rotation of cutting parts 1 and 2 but in different directions. If the frequency of the load is equal to the natural frequency of a specific order, it will cause the vibration of that mode.

3. Cutting Load

3.1. DEM-MBD Bidirectional Coupling Simulation.

The excavation process of a bolter miner is a result of multiple coupling factors. The working mechanism parameters, kinematic parameters, rock properties of the material, and interaction between the cutting head and tunnel directly or indirectly influence the excavation process and dynamics of the bolter miner. Therefore, based on the principle of bidirectional coupling of DEM-MBD, a bidirectional coupling model was established using EDEM and RecurDyn software, as shown in Figure 2. The contact model between the coal and the cutting head was the Hertz–Mindlin (no-slip) contact model, with the contact parameters listed in Table 5 [15]. The contact model between coal particles is the Hertz–Mindlin model with bonding [16]. The particle adhesion parameters are listed in Table 6 [17].

3.2. Results.

Feed hollowing and downward cutting stages are the main stages of the cutting operation process and account for most of the working time [18]. Therefore, only the above two stages are considered for the simulation process.

The loads on the cutting head are mainly the combined forces F_x and F_y in x and y directions and the moment M on the z-axis of the cutting head. As shown in Figure 3(a), the external forces acting on the cutting head fluctuate owing to the random filling of the coal seam particles. During the hollowing stage, the loads increased with depth and reached their maximum values at a depth of 500 mm. During the cutting stage, the loads fluctuated steadily with amplitudes lower than those during the hollowing stage because the

TABLE 3: Main parameters of the bolter miner.

Parameters	Values
m_b	71000 kg
m_{c1}	1630 kg
m_{c2}	17000 kg
I_b	571321 kg m^2
I_{c1}	463 kg m^2
I_{c2}	8350 kg m^2
k_{by1}	8.9×10^9 N/m
k_{by2}	1.1×10^{10} N/m
k_{bx}	8.2×10^9 N/m
k_{c1}	2.3×10^8 N/m
k_{c2}	9.5×10^7 Nm/rad
c_{by1}	7.4×10^6 N·s/m
c_{by2}	9.7×10^6 N·s/m
c_{bx}	2×10^7 N·s/m
c_{c1}	2×10^5 N·s/m
c_{c2}	1.3×10^4 N·s/m
l_{b1}	2.8 m
l_{b2}	1.7 m
l_{b3}	0.8–1.8 m
l_{b4}	0.1 m–1.1 m
l_{c1}	2.1 m
l_{c2}	2.1 m
l_{cm}	0.8 m
φ_1	0°–25°
φ_2	22.5°–46°

cutting depths were less than those during the hollowing stage. As shown in Figure 3(b), the frequency-domain characteristics of the load in different directions were similar. It has a higher amplitude, below 8 Hz and approximately 23 Hz.

The external force vector Q acting on the five-degree-of-freedom model shown in Figure 1 can be expressed as follows:

$$Q = \begin{bmatrix} 0 \\ 0 \\ 0 \\ 0 \\ M + F_x l_{cb} \sin \varphi_1 + F_x l_{cb} \cos \varphi_1 \end{bmatrix}, \tag{5}$$

where l_{cb} is the distance between the center of mass of the cutting head and hinge point B.

4. Main Vibration Response Analysis of the System

4.1. Field Testing.

Vibration tests were conducted at the Hongliulin coal mine in Shanxi, China, to verify the accuracy of the dynamic model and determine the dominant vibration frequency of the cutting part of the bolter miner. The locations of the measurement and test sites are shown in Figure 4. Mounting an accelerometer on the cutting head is an ideal way to measure the vibration caused by the interaction between the cutting head and the coal tunnel. However, the environment in front of the cutting head is filled with rock fragments or mud, which can easily damage

TABLE 4: The five modes of the system.

Natural frequency (Hz)	Vibration shape
$\omega_1 = 4$ Hz	Cutting part 1 and cutting part 2 rotate in the same direction
$\omega_2 = 46.7$ Hz	Cutting part 1 and cutting part 2 rotate in the opposite direction
$\omega_3 = 47.5$ Hz	Main frame rotation
	Main frame translation in y direction
$\omega_4 = 63.8$ Hz	Cutting part 1 rotation
	Main frame translation in x direction
$\omega_5 = 84.6$ Hz	Cutting part 1 rotation
	Main frame translation in y direction
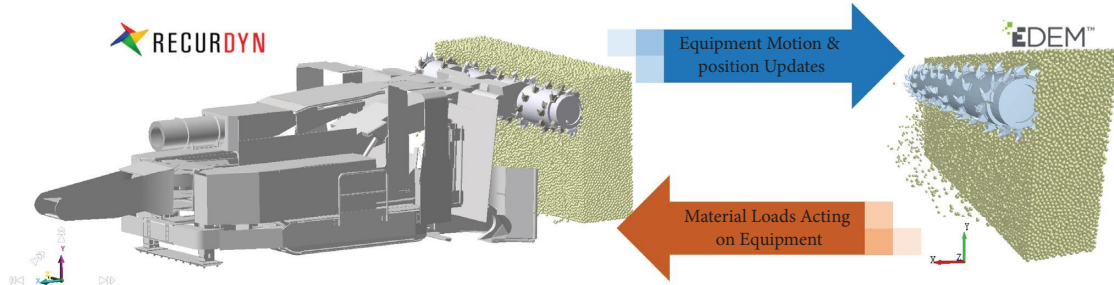
FIGURE 2: Bidirectional coupling simulation.

TABLE 5: The parameters of contact properties of coal and cutting head.

Materials parameters	Coefficient of restitution	Coefficient of static friction	Coefficient of rolling friction
Coal to coal	0.5	0.6	0.05
Coal to cutting head	0.5	0.4	0.05

TABLE 6: Particle adhesion parameters.

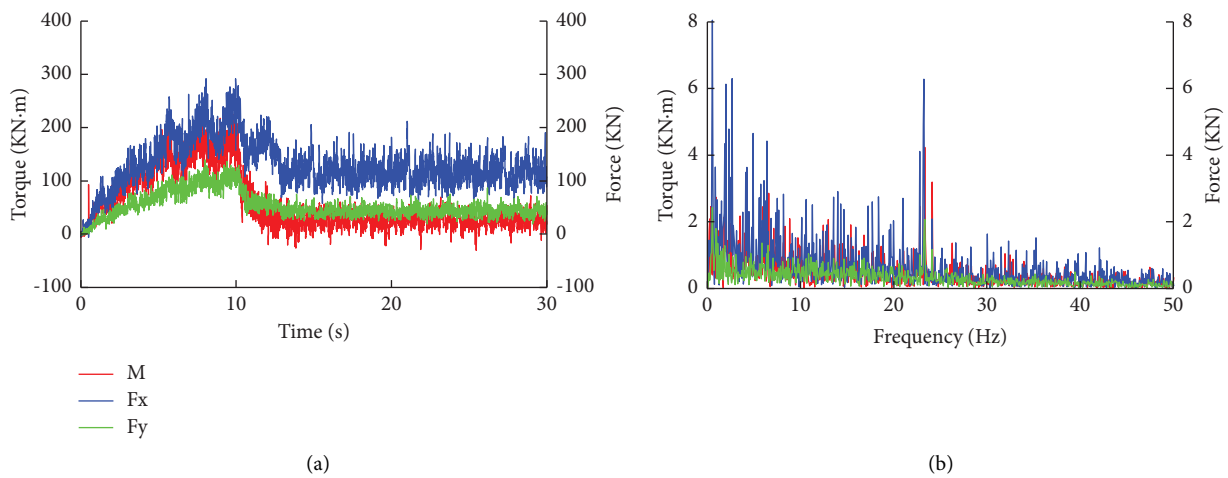| Normal stiffness (N/m³)	Tangential stiffness (N/m³)	Normal maximum stress (Pa)	Tangential maximum stress (Pa)	Bond disk radius (mm)
4.5×10^{10}	1.8×10^{10}	3.2×10^{6}	3×10^{6}	28

(a)

(b)

FIGURE 3: Cutting load. (a) Time domain. (b) Frequency domain.

the accelerometer. As shown in Figure 4(d), the inner wall of the cutting arm is the ideal measurement point for obtaining vibration signals from the cutting part. This location allows for a stable mounting of the accelerometer and protects it from damage. In addition, the accelerometer was covered with a waterproof film to prevent water from entering the cutting arm and damaging the accelerometer. Another measurement point was mounted at the rear of the machine to reflect the vibration characteristics of the main frame, as shown in Figure 4(c). Both accelerometers were magnetically mounted on a bolter miner.

4.2. Results. The load from Figure 3 is substituted into the bolter miner dynamics (1) to obtain the response at the corresponding position of the measurement point. The calculated results were compared with the measured results, as shown in Figure 5. The acceleration at measurement point 2 is much larger than that at measurement point 1, indicating a large attenuation of the vibration after it is transmitted to the main frame. The calculated time-domain response is close to the experimental results. The error of the RMS value of acceleration at measurement point 1 is within 7%, and the error of the measurement point 2 is within 4%. The primary frequencies of the vibration data of the cutting part are concentrated around 4 Hz and 23.3 Hz, and the

frequency distribution of the system vibration calculated by the dynamics model is in good agreement with the measured data, indicating that the model can describe the actual vibration of the system in the frequency domain more accurately. 23.3 Hz is the same as the frequency component of the cutting load, which is the forced vibration due to the excitation of the cutting head. According to the modal analysis in Section 2.2, 4 Hz is its first mode of vibration, and the low-frequency vibration around this frequency accounts for the most significant proportion of the vibration in the cutting part. This frequency is in the human body's sensitive frequency range, so this frequency is the primary consideration in the DVA design.

5. Bolter Miner with DVA

5.1. Equations of Motion in the Presence of DVA. It was assumed that the dynamic absorber was always inside the cutting arm, as shown in Figure 6. This is a typical choice in similar studies [14, 19] and is also convenient in practice because the interior of the cutting arm provides sufficient space for the DVA to move. Specifically, the DVA acts in the x1 direction when the system vibrates under a cutting load. The mass, stiffness, and damping matrices in (1) are converted into the 6×6 form.

$$\mathbf{M} = \begin{vmatrix} m_b + m_{c1} + m_{c2} & 0 & 0 & m_{c1}l_{cm}\sin\varphi_1 + m_{c2}l_{c1}\sin\varphi & m_{c2}l_{c2}\sin\varphi_1 & 0 \\ 0 & m_b + m_{c1} + m_{c2} & m_{c1}l_{b4} + m_{c2}l_{b4} & m_{c1}l_{cm}\cos\varphi_1 + m_{c2}l_{c1}\cos\varphi & m_{c2}l_{c2}\cos\varphi_1 & 0 \\ 0 & m_{c1}l_{b4} + m_{c2}l_{b4} & I_b + m_{c1}l_{b4}^2 + m_{c2}l_{b4}^2 & m_{c1}l_{b4}l_{c1}\cos\varphi_1 + m_{c2}l_{b4}l_{c1}\cos\varphi_1 & m_{c2}l_{b4}l_{c2}\cos\varphi_1 & 0 \\ m_cl_{cm}\sin\varphi_1 + m_{c2}l_{c1}\sin\varphi_1 & m_cl_{cm}\cos\varphi_1 + m_{c2}l_{c1}\cos\varphi_1 & m_{c1}l_{b4}l_{c1}\cos\varphi_1 + m_{c2}l_{b4}l_{c1}\cos\varphi_1 & I_{c1} + m_{c1}l_{cm}^2 + m_{c2}l_{c1}^2 & m_{c2}l_{c1}l_{c2} & 0 \\ m_{c2}l_{c2}\sin\varphi_1 & m_{c2}l_{c2}\cos\varphi_1 & m_{c2}l_{b4}l_{c2}\cos\varphi_1 & m_{c2}l_{c1}l_{c2} & I_{c2} + m_{c2}l_{c2}^2 & 0 \\ 0 & 0 & 0 & 0 & 0 & m_d \end{vmatrix}, \quad (6)$$

$$\mathbf{K} = \begin{vmatrix} \dfrac{k_d}{\sin^2\varphi_1} + k_{bx} & 0 & 0 & \dfrac{k_dl_{c1}}{\sin\varphi_1} & \dfrac{k_dl_d}{\sin\varphi_1} & -\dfrac{k_d}{\sin\varphi_1} \\ 0 & k_{by1} + k_{by2} & k_{by2}l_{b2} - k_{by1}l_{b1} & 0 & 0 & 0 \\ 0 & k_{by2}l_{b2} - k_{by1}l_{b1} & k_{by2}l_{b2}^2 + k_{by1}l_{b1}^2 + k_{c1}(l_{b4} - l_{b3})^2\cos^2\varphi_2 & k_{c1}(l_{b4} - l_{b3})l_{c1}\cos(\varphi_1 + \varphi_2) & 0 & 0 \\ \dfrac{k_dl_{c1}}{\sin\varphi_1} & 0 & k_{c1}(l_{b4} - l_{b3})l_{c1}\cos(\varphi_1 + \varphi_2) & k_{c1}l_{c1}^2\cos^2(\varphi_1 + \varphi_2) + k_{c2} + k_dl_{c1}^2 & -k_{c2} + k_dl_{c1}l_d & -k_dl_{c1} \\ \dfrac{k_dl_d}{\sin\varphi_1} & 0 & 0 & -k_{c2} + k_dl_{c1}l_d & k_{c2} + k_dl_d^2 & -k_dl_d \\ -\dfrac{k_d}{\sin\varphi_1} & 0 & 0 & -k_dl_{c1} & -k_dl_d & k_d \end{vmatrix}, \quad (7)$$
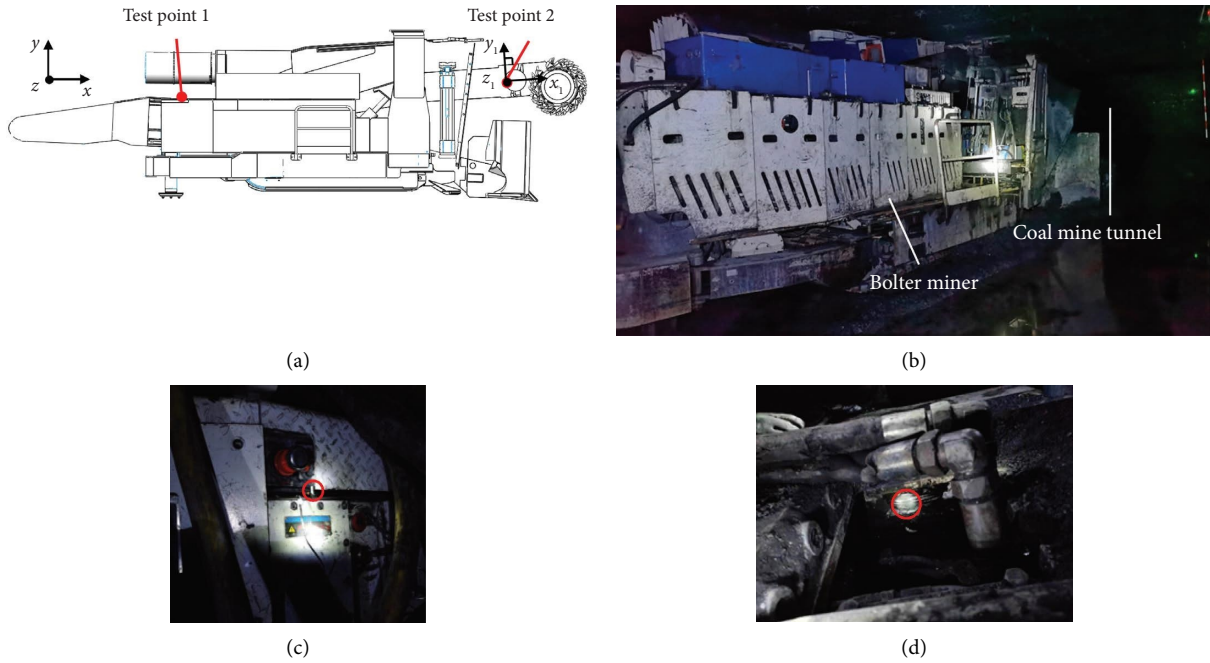
(a)

(b)

(c)

(d)

FIGURE 4: Acceleration field test. (a) Layout of test point arrangement. (b) Test site. (c) Test point 1. (d) Test point 2.
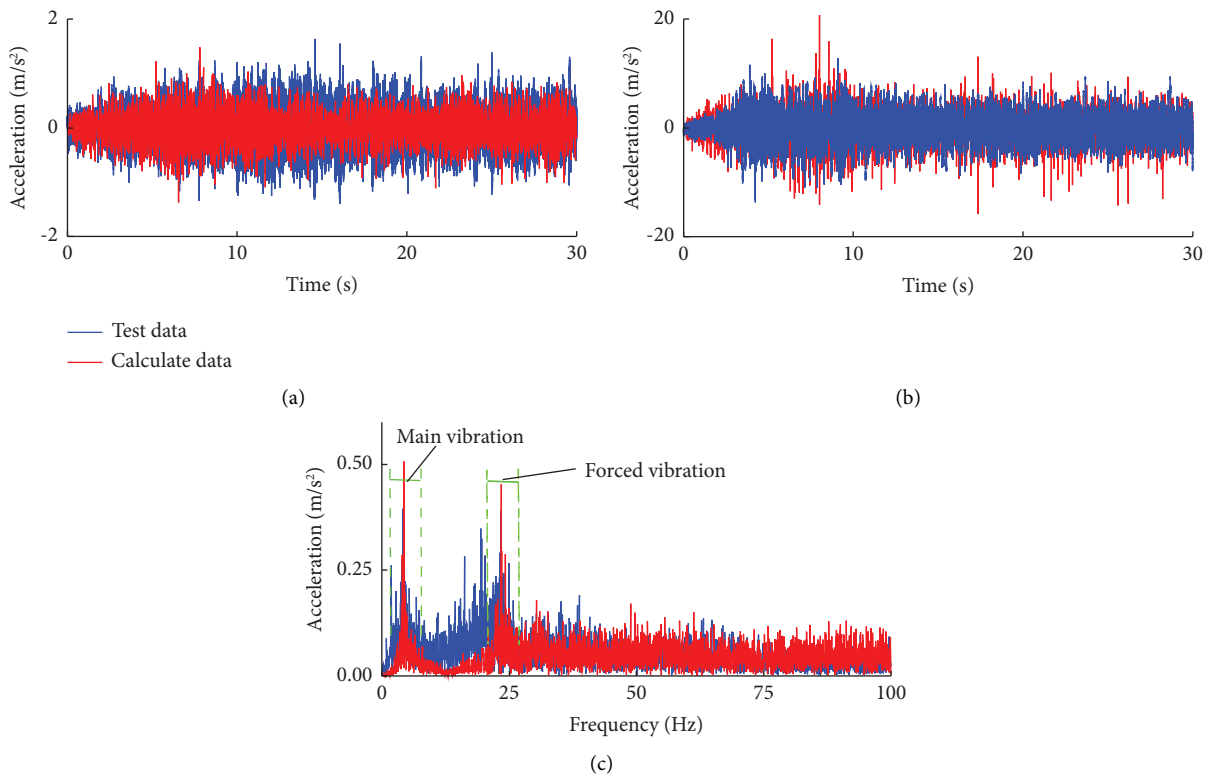

(a)

(b)

(c)

FIGURE 5: Test and calculate the acceleration response. (a) Acceleration of measurement point 1. (b) Acceleration of measurement point 2. (c) Frequency domain response of the acceleration of measurement point 2.
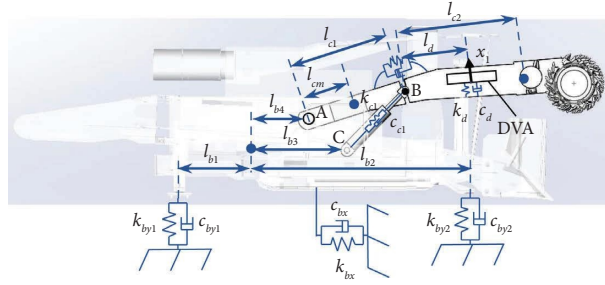
FIGURE 6: Bolter miner installed with DVA located in the cutting arm.

$$\mathbf{C} = \begin{vmatrix} \dfrac{c_d}{\sin^2\varphi_1} + k_{bx} & 0 & 0 & \dfrac{c_d l_{c1}}{\sin\varphi_1} & \dfrac{c_d l_d}{\sin\varphi_1} & -\dfrac{c_d}{\sin\varphi_1} \\[2mm] 0 & c_{by1} + c_{by2} & c_{by2}l_{b2} - c_{by1}l_{b1} & 0 & 0 & 0 \\[2mm] 0 & c_{by2}l_{b2} - c_{by1}l_{b1} & c_{by2}l_{b2}^2 + c_{by1}l_{b1}^2 + c_{c1}(l_{b4}-l_{b3})^2\cos^2\varphi_2 & c_{c1}(l_{b4}-l_{b3})l_{c1}\cos(\varphi_1+\varphi_2) & 0 & 0 \\[2mm] \dfrac{c_d l_{c1}}{\sin\varphi_1} & 0 & c_{c1}(l_{b4}-l_{b3})l_{c1}\cos(\varphi_1+\varphi_2) & c_{c1}l_{c1}^2\cos^2(\varphi_1+\varphi_2) + c_{c2} + c_d l_{c1}^2 & -c_{c2} + c_d l_{c1} l_d & -c_d l_{c1} \\[2mm] \dfrac{c_d l_d}{\sin\varphi_1} & 0 & 0 & -c_{c2} + c_d l_{c1} l_d & c_{c2} + c_d l_d^2 & -c_d l_d \\[2mm] -\dfrac{c_d}{\sin\varphi_1} & 0 & 0 & -c_d l_{c1} & -c_d l_d & c_d \end{vmatrix}, \tag{8}$$

where m_d, k_d, and c_d are the mass, stiffness, and damping coefficients of DVA, respectively. l_d is the distance between the hinge point B and the center of mass of the DVA.

Correspondingly, the external force vector Q is expressed as follows:

$$Q = \begin{vmatrix} 0 \\ 0 \\ 0 \\ 0 \\ M + F_x l_{cb}\sin\varphi_1 + F_x l_{cb}\cos\varphi_1 \\ 0 \end{vmatrix}. \tag{9}$$

It is important to emphasize that the installation of the DVA does not affect the stability of the bolter miner operation or the position of the center of mass, as the mass of the selected DVA is small compared to the total mass.

5.2. DVA Parameter Optimization

5.2.1. Objective Function. According to equations (6)–(8), it can be seen that the bolter miner has a variety of characteristics due to the different DVA parameters such as mass, stiffness, damping, and layout position, so it is necessary to optimize the DVA parameters in order to achieve the most effective vibration reduction performance.

Since the cutting arm pitch vibration is the source of extra cutting fatigue load [20], the performance index J_{16} is defined as follows:

$$J_1 = \frac{\max\left(\left|H_{F \longrightarrow (\theta_{c2}-\theta_{c1})}\right|_{w/\mathrm{DVA}}\right)}{\max\left(\left|H_{F \longrightarrow (\theta_{c2}-\theta_{c1})}\right|_{w/o\mathrm{DVA}}\right)}, \tag{10}$$

where $\theta_{c2} - \theta_{c1}$ represents the relative rotational displacement of the cutting arm; $H_{F \longrightarrow (\theta_{c2}-\theta_{c1})}$ is the frequency response function from the cutting load to the relative displacement of the cutting arm, w/DVA means a DVA is installed, and $w/o\mathrm{DVA}$ means a DVA is not installed.

The y-direction motion of the main frame can reflect the vibration intensity of the main frame, and the performance index J_2 can be expressed as follows:

$$J_2 = \frac{\max\left(\left|H_{F \longrightarrow y}\right|_{w/\mathrm{DVA}}\right)}{\max\left(\left|H_{F \longrightarrow y}\right|_{w/o\mathrm{DVA}}\right)}, \tag{11}$$

where $H_{F \longrightarrow y}$ is the frequency response function from the cutting load to the displacement of the main frame along the y-axis.

For indices J_1 and J_2, a value less than 1 means that the controlled system has a smaller response than the uncontrolled system. The objective function was constructed using these two performance indices.

$$\min\left\{J = \frac{1}{2}J_1 + \frac{1}{2}J_2\right\}. \tag{12}$$

5.2.2. Modeling for the TMD Displacement Limitation. Due to the limited space of the cutting arm, it is necessary to set a stop to prevent the DVA stroke from exceeding the limitation. According to the dimensions of the cutting

arm, the allowable stroke ranges of the DVA are designated as ±0.06 m. When the DVA reaches the limiting position, the stopping force is added to the DVA, and a reaction force acts on the cutting arm. Otherwise, the stopping force F_{stop} equals zero, as represented in the following equation:

$$F_{stop} = \begin{cases} 0, & |x_1| < L, \\ -K_{stop} \cdot \Delta x_1, & (x_1 \geq L \cap \dot{x}_1 \leq 0) \cup (x_1 \leq L \cap \dot{x}_1 \geq 0), \\ -K_{stop} \cdot \Delta x_1 - C_{stop} \cdot \dot{x}_1, & (x_1 \geq L \cap \dot{x}_1 > 0) \cup (x_1 \leq L \cap \dot{x}_1 < 0), \end{cases} \tag{13}$$

where K_{stop} and C_{stop} are the stop stiffness and damping coefficients, respectively, with values of 1×10^7 N/m and 1×10^7 N s/m; L is the maximum allowable stroke length; Δx_1 is the distance that the DVA traveled beyond the allowable stroke length.

5.2.3. Optimization Results. Among the parameters of the DVA, the mass md and the layout position ld are constrained by the structure of the cutting arm. First analyze the effect of mass on the performance of DVA, and let l_d is equal to 1.5 m. The masses of 500, 1000, 1500, and 2000 kg are selected, and the optimization method is chosen as the genetic algorithm. The optimization results and performance indices are shown in Table 7. When the mass increases from 500 to 2000, the performance index J_1 decrease from 0.78 to 0.64 and J_2 decreases from 0.81 to 0.63. This indicates that the higher the mass of the DVA, the better its performance. However, excessive weight will cause DVA installation and repair difficult, so a mass of 1638 kg is chosen. The density of the oscillator material is 7800 kg/m³, and the dimensions of the DVA oscillator are designed as $1000 \times 700 \times 300$ mm.

After determining the mass of the DVA, it is necessary to analyze the effect of the DVA layout location on its performance. We chose three possible layout positions: 0.5, 1, and 1.5 m. The performance indices of different layout positions are shown in Table 8. When the layout location increases from 0.5 to 1.5, the performance index J_1 decreases from 0.74 to 0.65 and J_2 decreases from 0.74 to 0.66. This indicates that the larger the l_d, the better the DVA performance and hence $l_d = 1.5$ is chosen. On the other hand, when the mass is defined, the optimization results for stiffness and damping coefficients are kept constant. Finally, the performance parameters of DVA were determined, as shown in Table 9.

6. Results and Analysis

6.1. Frequency Response. The frequency response curves of the cutting load to the relative displacement of the cutting part and main frame displacement in the y-axis after the installation of DVA are calculated and shown in Figure 7. For the frequency response function $H_{F \longrightarrow (\theta_{c2} - \theta_{c1})}$, the first-order resonance peaks are significantly suppressed. However, new resonance frequencies appear at 3.4 Hz and 4.6 Hz, which are much lower than the original peaks due to damping, and the resonance peaks are reduced by 35% with DVA compared without DVA. For the $H_{F \longrightarrow y}$, new resonance frequencies appear on both sides of the original resonance frequency, and the resonance peak decays by 34%.

6.2. Time Domain. The loads in Figure 3 are used as excitations to calculate the dynamic response of the bolter miner with DVA, as shown in Figure 8. The vibration acceleration amplitude of both the cutting part and the main frame was reduced. The acceleration RMS and peak values of the cutting part with DVA were reduced by 12% and 30.1%, respectively. The acceleration RMS and peak values of the main frame with DVA were reduced by 6.5% and 17%, respectively.

The dynamic response of the DVA oscillator is extracted to judge whether it satisfies the displacement constraints and to verify its vibration absorption mechanism. According to Figure 9, the maximum displacement of the DVA vibrator is 0.058 m, which is within the displacement constraints. The vibration of the oscillator is more severe under external load excitation, while the main frequency of its vibration is concentrated around 4 Hz, which indicates that the DVA resonates under the vibration of the cutting arm and absorbs the vibration energy of the main system to the maximum extent, so that the vibration of the main system is minimized.

6.3. Cutting Arm Fatigue Analysis. Fatigue failure is caused by the accumulated damage on the surface of the member under alternating external loads [21]. To analyze the effect of installing DVA on the fatigue life of the cutting arm, the cutting arm was modeled as a flexible body, and the damage on the surface of the unit was analyzed using the finite element method. Figure 10 shows the cutting process after replacing the cutting arm with a flexible body.

The linear fatigue damage theory (Palmgren–Miner criterion) was used to calculate the total damage and fatigue life of the cutting arm [22, 23]. Figure 11(a) shows the life contour of the cutting arm without the DVA installed; the minimum life is shown in red, and the maximum life is shown in blue. The minimum node of the cutting arm cycle number was 2532, and the cycle number was 1.7305e6, which was located at the rear of the cutting arm, the area where the cross-sectional shape of the cutting arm changes, and the fatigue damage value was 5.7787e − 7. The lifetime of the area where the ear base and cutting arm are connected is relatively short. The actual crack location is consistent with

TABLE 7: Optimization results and performance indices of different masses.

Masses (kg)	Stiffness (N/m)	Damping (N·s/m)	J_1	J_2
500	3.28×10^5	9.10×10^2	0.78	0.81
1000	6.52×10^5	2.57×10^2	0.71	0.73
1500	9.71×10^5	4.71×10^2	0.67	0.67
2000	1.29×10^6	7.25×10^3	0.64	0.63

TABLE 8: Optimization results and performance indices of different layout positions.

Layout positions (m)	Stiffness (N/m)	Damping (N·s/m)	J_1	J_2
0.5	1.06×10^5	5.38×10^3	0.74	0.74
1	1.06×10^5	5.38×10^3	0.70	0.69
1.5	1.06×10^5	5.38×10^3	0.65	0.66

TABLE 9: DVA parameters.

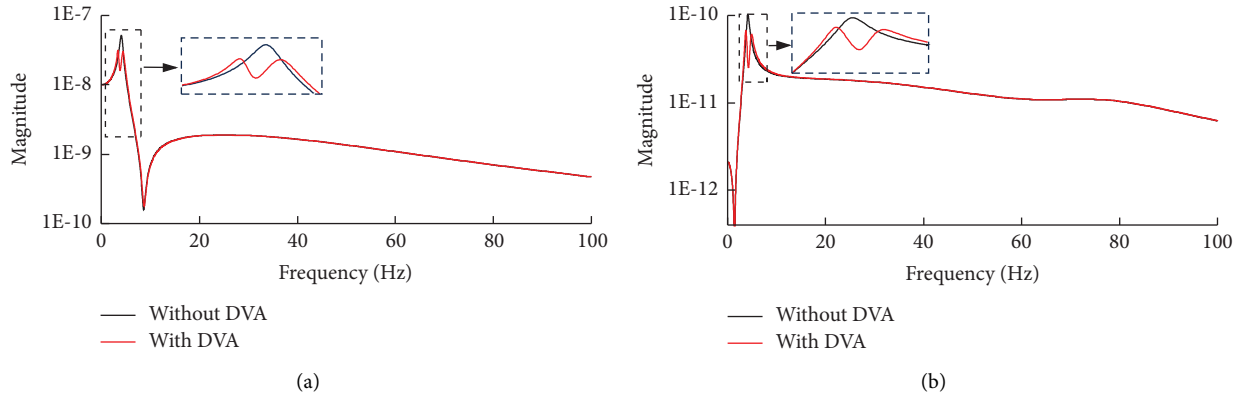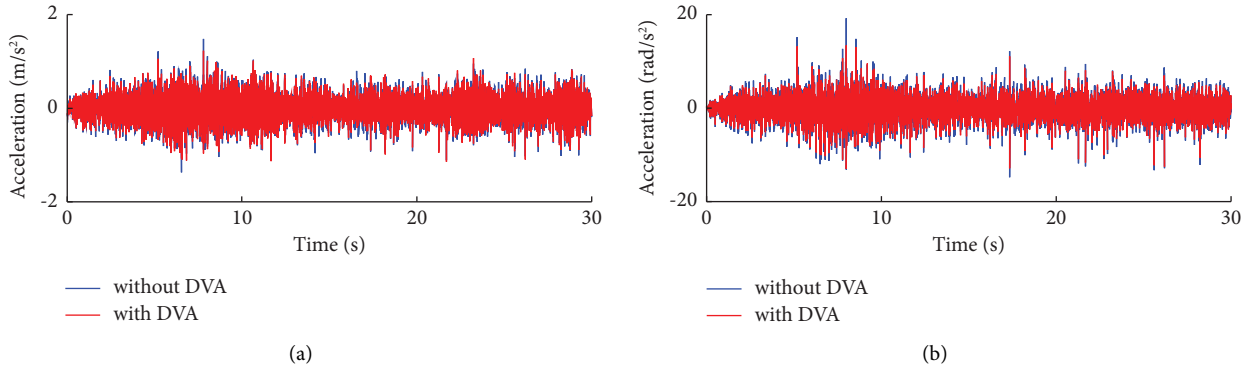| Parameters	Values
m_d (kg)	1638
k_d (N/m)	1.06×105
c_d (N·s/m)	5.38×103
Dimension (mm)	$1000 \times 700 \times 300$
Layout position (m)	1.5

(a)

(b)

FIGURE 7: Frequency response curve. (a) $H_{F \longrightarrow (\theta_{c2} - \theta_{c1})}$. (b) $H_{F \longrightarrow y}$.

(a)

(b)

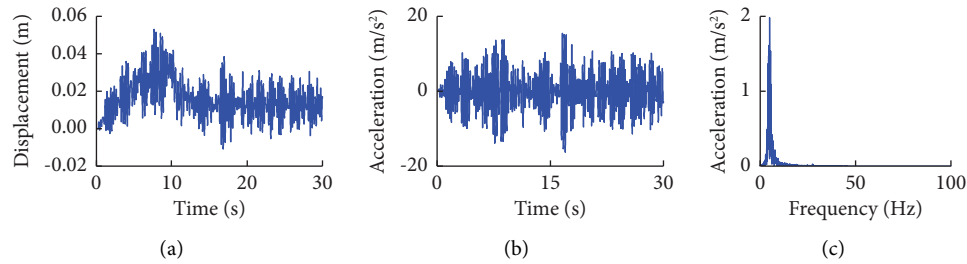FIGURE 8: Vibration response. (a) Cutting part vibration. (b) Main frame.

Figure 9: DVA oscillator response. (a) Displacement. (b) Acceleration. (c) Frequency domain.
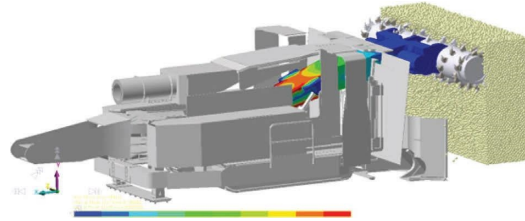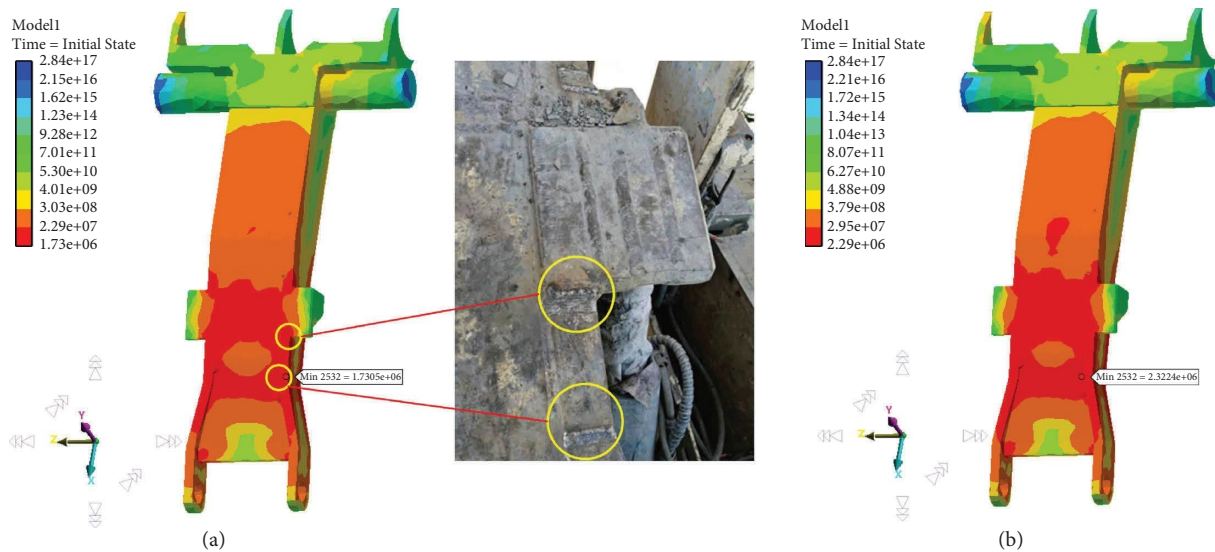

Figure 10: Simulation process.

Figure 11: Cutting arm life contour. (a) Without DVA and actual fatigue damage location. (b) With DVA.

the simulation results, which verifies the reasonableness and feasibility of the fatigue analysis method.

As shown in Figure 11(b), the minimum number of cycles increased to 2.3224e6 with the DVA, and the fatigue life increased by 34.2%. This is because the pitch vibration of the cutting arm is the source of the fatigue load, and the DVA reduces the amplitude of the cutting arm, thus reducing the load and fatigue and reducing the potential maintenance cost.

7. Conclusions

This paper performed multibody dynamics modeling and vibration suppression with a passive DVA for an EJM340-type bolter miner. First, the multibody dynamics model of the bolter miner was established, the modal vibration pattern was obtained, and the cutting load was obtained based on the discrete element method. Second, field tests were conducted to verify the model's accuracy and determine the main vibration frequency. Subsequently, a coupling model between the bolter miner and the DVA was established, and the parameters of the DVA were optimized. Lastly, to evaluate the DVA, the vibration suppression effect and the effect on fatigue life were analyzed separately. The results show a good vibration suppression effect on both the main frame and the cutting part, which prolongs the fatigue life of the cutting arm and has a positive effect on the protection of the operator and the reliability of the equipment. It should be noted that the influence of gangue and fault is not considered in the tunnel model, resulting in some errors in the

calculation results, so further analysis should be carried out in the following work for the vibration under complex working conditions. Passive DVA is used in this study, and semiactive and active DVA are also worth studying.

Data Availability

All the data generated or analyzed during this study are included within this article.

Conflicts of Interest

The authors declare that they have no conflicts of interest.

Acknowledgments

References

[1] S. Deshmukh, A. K. Raina, V. Murthy, R. Trivedi, and R. Vajre, "Roadheader- a comprehensive review," *Tunnelling and Underground Space Technology*, vol. 95, Article ID 103148, 2020.

[2] P. Ma, D. Qian, N. Zhang, H. Shimada, D. Pan, and K. Huang, "Application of bolter miner rapid excavation technology in deep underground roadway in inner Mongolia: a case study," *Sustainability*, vol. 12, no. 7, p. 2588, 2020.

[3] Z. Tian, S. Gao, S. X. Jing, and J. Li, "Reliability and fatigue life analysis of key parts of shearer," *Engineering Failure Analysis*, vol. 138, Article ID 106357, 2022.

[4] P. Cheluszka, "The anti-resonance criterion in selecting PICK systems for fully operational cutting machinery used in mining," *Archives of Mining Sciences*, vol. 62, no. 4, pp. 775–793, 2017.

[5] A. Mezyk, W. Klein, M. Pawlak, and J. Kania, "The identification of the vibration control system parameters designed for continuous miner machines," *International Journal of Non-linear Mechanics*, vol. 91, pp. 181–188, 2017.

[6] R. Ibrahim, "Recent advances in nonlinear passive vibration isolators," *Journal of Sound and Vibration*, vol. 314, no. 3-5, pp. 371–452, 2008.

[7] S. Wu and H. Li, "A data-driven design method of distributed dynamic vibration absorber for broadband vibration suppression of thin-walled structures," *Thin-Walled Structures*, vol. 182, Article ID 110264, 2023.

[8] E. Barredo, J. Mendoza Larios, J. Colín, J. Mayén, A. Flores-Hernández, and M. Arias-Montiel, "A novel high-performance passive non-traditional inerter-based dynamic vibration absorber," *Journal of Sound and Vibration*, vol. 485, Article ID 115583, 2020.

[9] Z. Lu, Z. Wang, Y. Zhou, and X. Lu, "Nonlinear dissipative devices in structural vibration control: a review," *Journal of Sound and Vibration*, vol. 423, pp. 18–49, 2018.

[10] F. Weber, P. Huber, F. Borchsenius, and C. Braun, "Performance of TMDI for tall building damping," *Actuators*, vol. 9, no. 4, pp. 139–213, 2020.

[11] Z. Lu, X. Lu, W. Lu, and S. F. Masri, "Experimental studies of the effects of buffered particle dampers attached to a multi-degree-of-freedom system under dynamic loads," *Journal of Sound and Vibration*, vol. 331, no. 9, pp. 2007–2022, 2012.

[12] K. M. Shum, "Closed form optimal solution of a tuned liquid column damper for suppressing harmonic vibration of structures," *Engineering Structures*, vol. 31, no. 1, pp. 84–92, 2009.

[13] M. Gutierrez Soto and H. Adeli, "Tuned mass dampers," *Archives of Computational Methods in Engineering*, vol. 20, no. 4, pp. 419–431, 2013.

[14] V. Laface, G. Alotta, G. Failla, C. Ruzzo, and F. Arena, "A two-degree-of-freedom tuned mass damper for offshore wind turbines on floating spar supports," *Marine Structures*, vol. 83, no. 7, Article ID 103146, 2022.

[15] J. Liu, C. Ma, Q. Zeng, and K. Gao, "Discrete element simulation of conical pick's coal cutting process under different cutting parameters," *Shock and Vibration*, vol. 2018, Article ID 7975141, 9 pages, 2018.

[16] X. Liu, X. Li, X. Fu, X. Yang, and J. Zhang, "Analysis on the influence law of traction speed on the cutting performance of coal containing hard concretion," *Mechanics & Industry*, vol. 24, no. 5, pp. 5–14, 2023.

[17] X. Yang, D. Wu, X. Zou, H. Chen, and S. Zhang, "An analysis of digging anchor machine stability and track wear under digging conditions," *Scientific Reports*, vol. 12, no. 1, Article ID 17738, 2022.

[18] Z. Xie, N. Zhang, D. Qian, C. Han, Y. An, and Y. Wang, "Rapid excavation and stability control of deep roadways for an underground coal mine with high production in Inner Mongolia," *Sustainability*, vol. 10, no. 4, p. 1160, 2018.

[19] V. Jahangiri and C. Sun, "Three-dimensional vibration control of offshore floating wind turbines using multiple tuned mass dampers," *Ocean Engineering*, vol. 206, Article ID 107196, 2020.

[20] A. Li, B. K. Wang, T. Wang, Z. F. Guo, and Z. K. Yan, "Effects of cutting head load on fatigue life of bolter miner cutting arm," *Mechanics & Industry*, vol. 24, no. 22, pp. 22–29, 2023.

[21] L. Pan, X. Guan, X. Luan et al., "Fatigue analysis of dozer push arms under tilt bulldozing conditions," *Machines*, vol. 10, no. 1, 2022.

[22] Y. Zhang, J. Chen, S. Hu, H. Zhang, and A. M. Kaynia, "Hysteretic damping of soils for well conductor fatigue analysis," *Marine Structures*, vol. 89, Article ID 103392, 2023.

[23] E. Santecchia, A. Hamouda, F. Musharavati et al., "A review on fatigue life prediction methods for metals," *Advances in Materials Science and Engineering*, vol. 2016, Article ID 9573524, 26 pages, 2016.